Materials Today Bio 29 (2024) 101319

Contents lists available at ScienceDirect

Materials Today Bio

journal homepage: www.journals.elsevier.com/materials-today-bio

Potential of a CO_2-Responsive supramolecular drug-carrier system as a safer and more effective treatment for cancer

Enyew Alemayehu Bayle [a,1], Fasih Bintang Ilhami [a,d,1], Jem-Kun Chen [c], Chih-Chia Cheng [a,b,*]

[a] Graduate Institute of Applied Science and Technology, National Taiwan University of Science and Technology, Taipei, 10607, Taiwan
[b] Advanced Membrane Materials Research Center, National Taiwan University of Science and Technology, Taipei, 10607, Taiwan
[c] Department of Materials Science and Engineering, National Taiwan University of Science and Technology, Taipei, 10607, Taiwan
[d] Department of Natural Science, Faculty of Mathematics and Natural Science, Universitas Negeri Surabaya, Surabaya, 60231, Indonesia

ARTICLE INFO

Keywords:
Cytosine
CO_2 responsiveness
Hypercapnic tumor microenvironment
Supramolecular drug-carrier system
Selective cellular uptake and cytotoxicity

ABSTRACT

We combined carbon dioxide (CO_2)-responsive cytosine-containing rhodamine 6G (Cy-R6G) as a hydrophobic anticancer agent with hydrogen-bonded cytosine-functionalized polyethylene glycol (Cy-PEG) as a hydrophilic supramolecular carrier to construct a CO_2-responsive drug delivery system, with the aim of enhancing the responsiveness of the system to the tumor microenvironment and thus the overall effectiveness of anticancer therapy. Due to self-complementary hydrogen bonding interactions between cytosine units, Cy-R6G and Cy-PEG co-assemble in water to form spherical-like nanogels, with Cy-R6G effectively encapsulated within the nanogels. The nanogels exhibit several distinctive physical features, such as widely tunable nanogel size and drug loading capacity for Cy-R6G, intriguing fluorescence properties, high co-assembled structural stability in normal aqueous environments, enhanced anti-hemolytic characteristics, sensitive dual CO_2/pH-responsive behavior, and precise and easily controllable CO_2-induced release of Cy-R6G. Cytotoxicity assays clearly indicated that, due to the presence of cytosine receptors on the surface of cancer cells, Cy-R6G-loaded nanogels exert selective cytotoxicity against cancer cells in pristine culture medium, but do not affect the viability of normal cells. Surprisingly, in CO_2-rich culture medium, Cy-R6G-loaded nanogels exhibit a further significant enhancement in cytotoxicity against cancer cells, and remain non-cytotoxic to normal cells. More importantly, a series of *in vitro* experiments demonstrated that compared to pristine culture medium, CO_2-rich culture medium promotes more rapid selective internalization of Cy-R6G-loaded nanogels into cancer cells through cytosine-mediated macropinocytosis and thus accelerates the induction of apoptosis. Therefore, this newly developed system provides novel avenues for the development of highly effective CO_2-responsive drug delivery systems with potent anticancer capabilities.

1. Introduction

Anti-cancer drugs play a crucial role in the treatment of cancer. The aim of using these drugs is to efficiently disrupt the uncontrolled growth of cancer cells, and ultimately inhibit the proliferation and ability of cancer cells to invade surrounding tissues [1,2]. Despite significant advancements in cancer research and drug development, anti-cancer drugs often lead to severe challenges such as toxicity and side effects [3,4]. Thus, many research teams have diligently worked to develop nano-carriers that stably encapsulate anti-cancer drugs and maximize therapeutic efficacy by specifically binding to target receptors on cancer cells, to minimize the adverse effects of chemotherapy in healthy tissues [5,6]. Among the numerous nano-carrier systems developed for drug delivery, supramolecular drug delivery systems (SDDs) have garnered significant interest as promising solutions to overcome the limitations of conventional chemotherapy [7–9]. In recent years, SDDs have emerged as potential drug delivery tools due to their ability to achieve precisely targeted drug release along various release profiles by adapting to changes in the surrounding environment, such as pH, temperature, glucose, light, and enzymes [10,11]. The unique physiological stimuli present in the tumor microenvironment compared to normal tissues have facilitated the application and effectiveness of SDDs in anticancer drug delivery [12]. By responding to changes in the tumor environment or external microenvironmental stimuli, SDDs can effectively achieve

* Corresponding author. Graduate Institute of Applied Science and Technology, National Taiwan University of Science and Technology, Taipei, 10607, Taiwan.
E-mail address: ccheng@mail.ntust.edu.tw (C.-C. Cheng).
[1] Both authors contributed equally to this work.

https://doi.org/10.1016/j.mtbio.2024.101319
Received 3 September 2024; Received in revised form 15 October 2024; Accepted 27 October 2024
Available online 29 October 2024

sustained or controlled intracellular drug release and thereby improve the overall therapeutic effects of anticancer drugs [12,13]. Therefore, SDDs are stimuli-responsive smart drug delivery materials that hold significant potential to achieve safer and more effective treatment strategies for cancer.

Excessive accumulation of carbon dioxide (CO_2) is the primary cause of tissue acidification in the tumor microenvironment. Compared to healthy tissues, where CO_2 levels are below 35 mmHg, a variety of tumor environments exhibit significantly higher CO_2 levels, ranging from 60 to 90 mmHg [14,15]. The presence of excess CO_2 leads to hypoxia and acidosis, which in turn contribute to the development of chemoresistance in cancer cells and exacerbate the progression of cancer, making it more difficult to treat the disease. In recent years, some studies have reported that reducing hypercapnia can mitigate chemoresistance in cancer cells and enhance therapeutic efficacy [16,17]. However, due to a lack of biological knowledge and the specific biocharacteristics of active gases, progress in using CO_2 as a trigger for drug delivery applications has been relatively slow [18,19]. However, despite numerous challenges and the lack of clarity on the related mechanisms, the advantages of CO_2 as an environmental trigger have garnered significant attention and driven the development of various CO_2-sensitive materials [20,21]. These materials typically contain functional groups that can react with CO_2, such as amidine, guanidine, amine, imidazole, and carboxyl groups [20,22]. Among their many exciting physical properties, the reversibility of CO_2-sensitive materials is particularly notable, as the materials can rapidly revert to their original state on bubbling with inert gases such as nitrogen (N_2) or argon [21]. Thus, we boldly hypothesize that targeting the high levels of CO_2 in the tumor microenvironment using the unique physical properties of CO_2-sensitive materials could provide a route to create CO_2-responsive SDDs with the potential to achieve precisely controlled drug release in hypercapnic (or CO_2-rich) tumor microenvironments and thereby enhance the safety and effectiveness of cancer treatment. This strategy may provide a reliable pathway to overcome numerous obstacles and challenges in drug delivery applications, including uncontrolled drug release behavior, non-selective cellular uptake, and severe adverse toxic effects in healthy tissues.

Rhodamine 6G (R6G) is a commercially available cationic water-soluble dye with distinctive fluorescent properties that has been extensively studied and utilized as a luminescent material [23,24]. Due to its high fluorescence quantum yield and stability, R6G has also been employed as a bioprobe in biomedical applications [25]. Moreover, Warner and co-workers successfully demonstrated that various functionalized R6G molecules exhibit cytotoxic activity against breast cancer cells [23,26]. Notably, these R6G derivatives are internalized by cancer cells through endocytosis and subsequently selectively induce cancer cell death, while causing minimal harm to healthy cells. Furthermore, due to their inherent fluorescent properties, the fluorescence distribution of R6G and its derivatives within cells can be monitored to confirm the pathways and mechanisms of cell killing [27]. However, before R6G can be safely and widely used as an anticancer agent in cancer therapy, several challenging limitations must be addressed. These limitations include the propensity of R6G to aggregate in aqueous environments due to its heterocyclic aromatic ring groups, high instability in biological environments, and inadequate selective uptake by cancer cells [28,29]. To address these complex issues, based on our previous developments and foundation in CO_2-responsive R6G [29] and nucleobase-functionalized SDDs [30–32], we reasonably speculated that cytosine molecules with self-complementary hydrogen bonding and cancer-targeting properties [32] could be conjugated separately to R6G and hydrophilic polyethylene glycol (PEG) through an appropriate synthetic approach to produce CO_2-responsive cytosine-containing R6G (Cy-R6G) and cytosine-functionalized PEG (Cy-PEG). In addition, based on our previous findings, the cytosine groups on the supramolecular nanogel structure exhibit a high affinity for the surface of cancer cells, thus resulting in a significant enhancement of cancer cell-specific uptake, increased cytotoxicity of anticancer drugs, and ultimately leading to a safer and more effective induction of cancer cell apoptosis [32]. Subsequently, due to hydrogen bonding interactions between the cytosine groups in both materials, the combination of Cy-R6G and Cy-PEG should form multifunctional assembled nanostructures in aqueous environments, which may confer highly sensitive CO_2-triggered drug release capability and ultimately provide a route to achieve highly targeted anticancer therapeutic efficacy in the hypercapnic tumor microenvironment.

In this study, we propose a potential strategy to enhance the efficacy of cancer treatment by targeting the hypercapnic tumor microenvironment through CO_2-responsive SDDs. Due to the self-complementary hydrogen bonding interactions between cytosine groups in both structures, pH-responsive cytosine-functionalized Cy-PEG as a hydrophilic nanocarrier and CO_2-sensitive cytosine-containing Cy-R6G as a hydrophobic anticancer agent can combine to form multifunctional co-assembled nanogels in aqueous solution (Scheme 1). Therefore, Cy-PEG can efficiently and stably encapsulate Cy-R6G and the amount of Cy-R6G encapsulated can be easily regulated based on the Cy-PEG to Cy-R6G mixing ratio. We demonstrate that the resulting nanogels exhibit several remarkable and unique physicochemical properties, such as intriguing emission phenomena, high structural stability in aqueous solutions, sensitive dual pH/CO_2 responsiveness, excellent anti-hemolytic activity, and precise CO_2-triggered drug release characteristics. More importantly, a series of *in vitro* cellular experiments conducted in CO_2-containing culture media confirmed that Cy-R6G-loaded Cy-PEG nanogels undergo significantly enhanced selective internalization into cancer cells, which is followed by rapid intracellular release of Cy-R6G that ultimately leads to massive levels of apoptosis within the cancer cells; however, Cy-R6G-loaded Cy-PEG does not affect normal cells. Therefore, these innovative SDDs provide valuable insight and establish a novel developmental framework for drug delivery applications that holds great potential to enhance the overall safety and efficacy of cancer treatment.

2. Experimental section

The experimental section in the *Supporting Information* includes details of the synthesis procedures, characterizations and analytical instruments, and cellular experiments.

3. Results and discussion

The core objective of this study was to establish a CO_2-responsive drug delivery system by integrating cytosine groups with targeting properties [32] into the structures of the carrier and the drug. We proposed that the intermolecular hydrogen bonding interactions and CO_2 sensitivity of cytosine moieties would enhance targeted delivery of the anticancer drug and trigger controlled intracellular drug release within the hypercapnic tumor microenvironment and thereby improve the overall safety, reliability, and efficacy of cancer treatment, as illustrated in Scheme 1. Water-soluble hydrogen-bonded cytosine-terminated Cy-PEG was obtained at high yield (85 %) through a one-pot Michael addition reaction between cytosine and PEG diacrylate (average molecular weight of 2000 g/mol) in the presence of a basic catalyst, as described in detail previously [30]. The resulting Cy-PEG exhibits high solubility in water and can spontaneously form self-assembled nanogels that effectively encapsulate hydrophobic anticancer agents, which may ultimately achieve stable drug delivery and controlled pH-induced drug release in the cellular environment [30]. Combination of the water-soluble cationic fluorescent dye R6G, which possesses ester reactive groups, with a cytosine derivative produces a cytosine-functionalized anticancer agent that is a new supramolecular fluorescent material. Cytosine-functionalized Cy-R6G was obtained through a facile and efficient two-step synthesis process, as shown in Scheme 1a. The primary amine cytosine derivative (Cy-amine) was

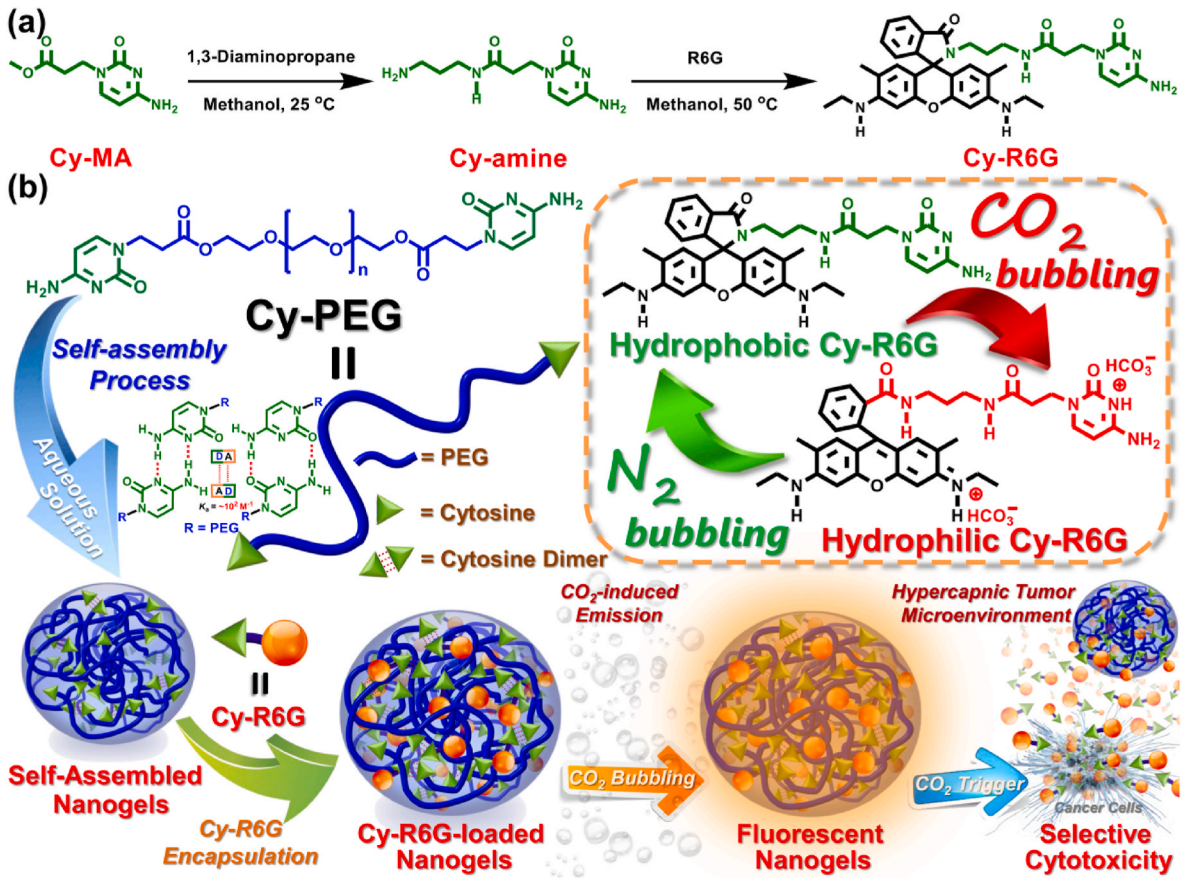

Scheme 1. **(a)** The two-step synthesis reaction used to prepare Cy-R6G. **(b)** Illustration of how the water-soluble supramolecular polymer Cy-PEG forms nanogels in water and encapsulates Cy-R6G through self-complementary hydrogen bonding cytosine interactions, exhibits changes in emission characteristics in response to CO_2 bubbling, rapidly releases Cy-R6G in a hypercapnic-like (CO_2-rich) cancer cell environment, and demonstrates selective cytotoxicity towards tumor cells. The diagram in the orange dashed framework on the right represents the structural transformation of Cy-R6G in response to CO_2 and N_2 bubbling.

obtained through a condensation reaction between methyl 3-(4-amino-2-oxopyrimidin-1(2H)-yl)propanoate (Cy-MA) [31] and an excess of 1,3-propanediamine (91 % yield). Subsequently, Cy-R6G was synthesized through a direct amidation reaction between Cy-MA and R6G at 55 °C without using a catalyst. During the amidation process, the aromatic amide intermediate undergoes further nucleophilic attack at the neighboring C9-position of the xanthene conjugation, leading to an intramolecular cyclization reaction [33,34] that results in the formation of a spirolactam functional group. Finally, after treatment and purification with chloroform and distilled water, pink Cy-R6G powder was successfully obtained at a yield of 88 %. The structure of Cy-R6G was confirmed using Fourier-transform infrared spectroscopy (FTIR), proton-1/carbon-13 nuclear magnetic resonance ($^{1}H/^{13}C$ NMR), high/low-resolution mass spectrometry, and elemental analysis (Figs. S1–S6 and Table S1, see supplementary data in the *Supporting Information*), which confirmed that the product obtained matched the expected structure. In addition, thermogravimetric analysis (TGA) indicated that due to the intermolecular hydrogen bonding interactions between the cytosine groups, Cy-R6G exhibits substantially higher thermal resistance with a decomposition temperature ($T_{d,5\ \%}$) of 297 °C compared to R6G ($T_{d,5\ \%}$ of 238 °C; Fig. S7). This significant enhancement in thermal stability demonstrates that the introduction of cytosine into the structure of R6G contributes to improve thermal stability, and further confirmed the successful synthesis of Cy-R6G through this efficient two-step synthetic route. Collectively, due to the presence of the cytosine groups in both structures, we anticipated that Cy-R6G would exhibit enhanced compatibility/affinity with Cy-PEG and stably load into the internal structure of self-assembled Cy-PEG nanogels in aqueous environments. Moreover, these features may confer cancer-targeting properties and responsiveness to the CO_2-rich tumor microenvironment, and thereby effectively enhance the efficacy of chemotherapy (Scheme 1).

Before assessing the behavior and physical characteristics of Cy-PEG nanogels encapsulating Cy-R6G, we first focused on the fundamental physical properties, pH and CO_2 responsiveness, and self-assembly behavior of Cy-R6G to establish a foundation and basis for subsequent investigation of Cy-R6G-loaded Cy-PEG nanogels. At 25 °C, Cy-R6G easily dissolves in various organic solvents (e.g., methanol, tetrahydrofuran, and chloroform), but is completely insoluble in aqueous solutions (even after heat treatment), indicating that the cytosine and spirolactam groups present in the structure of Cy-R6G significantly affect (or alters) its solubility in aqueous solutions compared to the highly water-soluble R6G. However, as the pH of the aqueous solution is gradually adjusted from 7.4 to 3.0, Cy-R6G progressively dissolves and changes the color of the solution, while the fluorescence intensity under broad-spectrum UV light gradually increases (as shown in the top and bottom photos of Fig. 1a). Notably, Cy-R6G completely dissolves at pH 3.0, forming a bright pink aqueous solution, suggesting that strong acid conditions effectively disrupt the self-complementary hydrogen bonds between the cytosine groups, and then rapidly react with the cytosine and spirolactam groups to form protonated cytosine and ring-opened spirolactam amide units that significantly enhance the solubility of Cy-R6G in water. Similar trends were observed in the ultra-violet visible (UV–Vis) and photoluminescence (PL) spectra. As the pH of the aqueous solution gradually decreased from 7.4 to 3.0, the maximum absorption peak intensity of Cy-R6G at 527 nm progressively increased (Fig. S8). Moreover, the intensity of the maximum emission peak increased from approximately 830 at pH 6.0 to over 8000 at pH 3.0 (under 525 nm

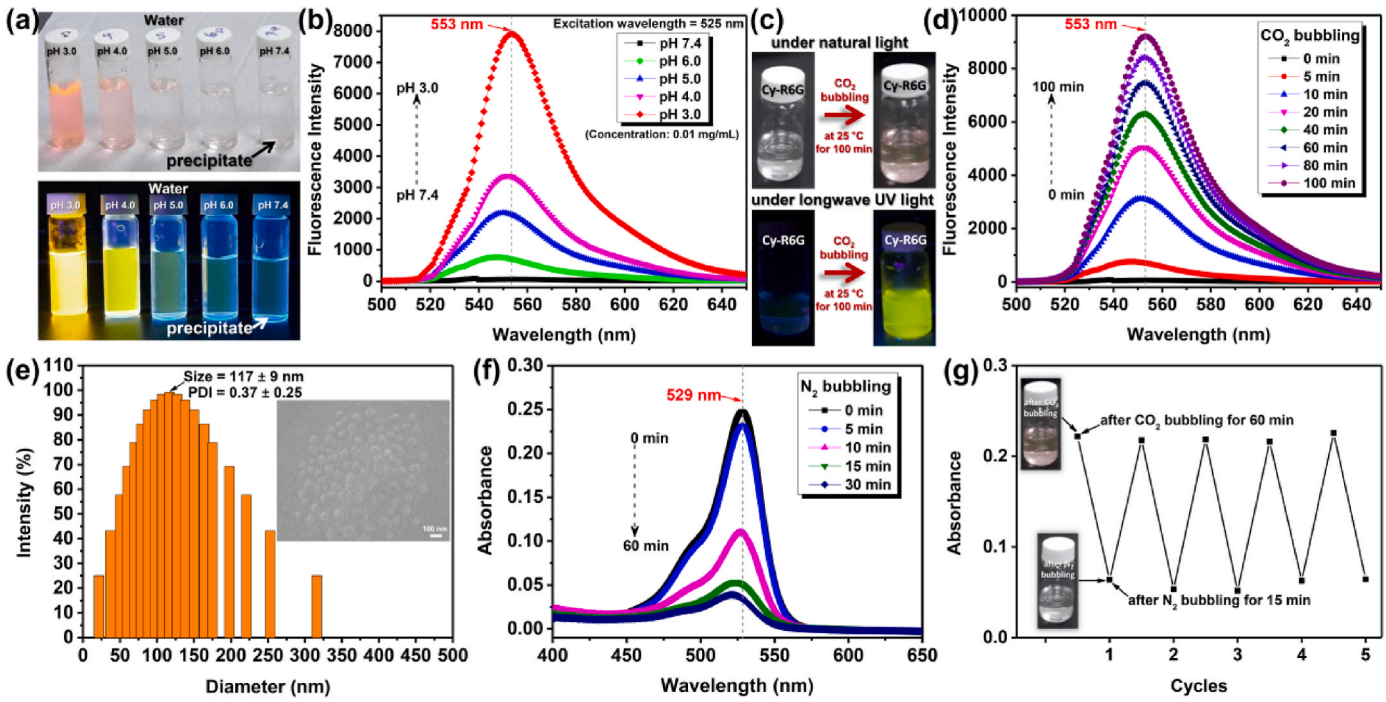

Fig. 1. **(a)** Photographs of Cy-R6G in aqueous solutions at different pH values at 25 °C under natural light (top) and long-wavelength UV light illumination (bottom). **(b)** PL spectra of Cy-R6G in aqueous solutions with pH values ranging from 7.4 to 3.0 at 25 °C. **(c)** Photographs of Cy-R6G in aqueous solution at 25 °C after CO_2 bubbling under natural light (top) and long-wavelength UV light illumination (bottom). **(d)** PL spectra of Cy-R6G in aqueous solution obtained over time at 25 °C after CO_2 bubbling for 0–100 min. **(e)** DLS curve of Cy-R6G in aqueous solution after CO_2 bubbling for 100 min at 25 °C. The inset at the top right shows a SEM image of Cy-R6G obtained after CO_2 bubbling treatment at 25 °C. **(f)** UV–Vis spectra of R6G-loaded Cy-PEG in aqueous solution obtained at 25 °C after different durations of N_2 bubbling (0–60 min). **(g)** Absorption intensity values of Cy-R6G in aqueous solution at 25 °C during five cycles of CO_2/N_2 alternate bubbling (established via UV–Vis spectroscopy). Each cycle lasted 75 min, with CO_2 bubbling for 60 min and N_2 bubbling for 15 min.

excitation wavelength) and its position also red-shifted from 546 nm to 553 nm (Fig. 1b). These phenomena can be attributed to protonation of the cytosine groups [35] and conversion of the spirolactam moieties from a non-fluorescent closed form to a fluorescent open form under acidic conditions [36], which effectively enhances the solubility and fluorescence properties of Cy-R6G in acidic aqueous environments. Thus, the presence of cytosine and spirolactam moieties confers Cy-R6G with unique pH-responsive and solubility/fluorescence-switching capabilities.

Cy-R6G is highly hydrophobic, which prevents changes in solubility and fluorescence in a normal physiological aqueous environment. Cytosine is a pyrimidine derivative that contains a nitrogen-containing heteroaromatic ring and amine and keto functional groups; its structure is similar to typical CO_2-reactive functional groups (e.g., imidazole, tertiary amines, amidines, and guanidines) [20]. Therefore, we anticipated that CO_2 bubbled into an aqueous suspension of Cy-R6G would react with the cytosine moieties and effectively transform hydrophobic Cy-R6G into a hydrophilic Cy-R6G with a structure incorporating ammonium bicarbonate groups, and thereby alter its water solubility and optical properties [29,37]. To validate this hypothesis, we investigated the effect of CO_2 bubbling on the solubility, optical absorption, and fluorescence properties of Cy-R6G in aqueous solution at 25 °C over time using digital photography, UV–Vis and PL spectroscopy. Surprisingly, in a 0.01 mg/mL aqueous suspension, Cy-R6G completely dissolved after 100 min of CO_2 bubbling and exhibited pink and yellow fluorescence under natural light and broad-spectrum UV light, respectively (Fig. 1c), suggesting that CO_2 effectively reacted with Cy-R6G to alter its solubility and emission properties in water. UV–Vis and PL further confirmed these macroscopic observations; as shown in Figs. S9 and 1d, the intensities of the maximum absorption and emission peaks (at 529 nm and 553 nm, respectively) of the 0.01 mg/mL Cy-R6G aqueous solution increased over time during continuous CO_2 bubbling for 100 min, reaching intensities of 0.26 and 9350 at 100 min. These observations indicate that the majority of the hydrophobic Cy-R6G had transformed into hydrophilic Cy-R6G containing cytosine combined with ammonium bicarbonate and an open-ring spirolactam group due to the CO_2-induced reaction and the influence of the resulting mildly acidic environment. Consequently, Cy-R6G became fully soluble in water and exhibited significantly enhanced fluorescence characteristics. In contrast, the positions and intensities of the maximum absorption and emission peaks of pristine water-soluble R6G showed almost no change after 100 min of CO_2 bubbling (Fig. S10), clearly revealing that the cytosine and spirolactam groups crucially endow Cy-R6G with its CO_2 responsiveness and fluorescence switching characteristics.

Measurements of pH and zeta potential (ζ) further validated these results: the pH and ζ values of unbubbled Cy-R6G aqueous solution were 7.09 ± 0.17 and -11.32 ± 2.67 mV, respectively. After 100 min of CO_2 bubbling, the pH of Cy-R6G aqueous solution decreased to 4.08 ± 0.13, while the ζ increased to 37.89 ± 1.87 mV. These results further confirmed that CO_2 bubbling induced the formation of charged bicarbonate groups in the structure of Cy-R6G, which thereby lowered the pH of the solution and subsequently transformed the closed-ring spironolactam group of Cy-R6G into a highly fluorescent open-ring form, resulting in an acidic, positively charged, homogenous fluorescent solution. Thus, a rapid transient reaction between CO_2 and the cytosine and amine moieties in Cy-R6G promotes structural transformation of Cy-R6G and confers a unique solubility change and fluorescence switching properties. These intriguing results prompted us to further explore the self-assembly structure of Cy-R6G in aqueous solution after 100 min of CO_2 bubbling using dynamic light scattering (DLS) at 25 °C and scanning electron microscopy (SEM). As shown in Fig. 1e, DLS indicated that CO_2-treated Cy-R6G in water formed a single distribution of nanoobjects with an average diameter of 117 ± 9 nm. This demonstrates that the CO_2-protonated cytosine and amine ion groups within the structure of Cy-

R6G (as depicted in the orange dashed frame on the upper right side of Scheme 1b) mutually repulse the adjacent hydrophobic heteroaromatic groups, and thus lead to generation of self-assembled nanostructures in water. SEM (right inset of Fig. 1e) revealed that CO_2-treated Cy-R6G exhibited spherical-like nanostructures with diameters of around 60–100 nm; this value is slightly smaller than the results obtained by DLS, possibly due to shrinkage of the nanoparticles upon drying [38]. Thus, the DLS and SEM observations clearly indicate that CO_2 bubbling can transform hydrophobic Cy-R6G into a water-soluble molecular structure that can self-assemble into spherical nanostructures. These results also further demonstrated that Cy-R6G not only possesses CO_2 responsiveness and undergoes acid-induced structural and fluorescence transformation behavior, but also exhibits unique self-assembly characteristics in aqueous environments [39].

Owing to its reversible solubility in water, CO_2-treated Cy-R6G can revert to its original hydrophobic state on bubbling the solution with non-reactive gases (such as N_2 or argon) or by increasing the ambient temperature [39,40]. Therefore, we investigated the rate and extent of CO_2 deprotonation of CO_2-treated Cy-R6G aqueous solution under N_2 bubbling at 25 °C and at different temperatures through UV–Vis spectroscopy. As expected, the maximum absorption peak at 529 nm for CO_2-treated Cy-R6G (i.e., the Cy-R6G solution after 100 min of CO_2 bubbling) decreased rapidly from approximately 0.25 to 0.04 after bubbling with N_2 for 60 min at 25 °C (Fig. 1f). This indicates that N_2 bubbling not only effectively removes CO_2 from the Cy-R6G structure, but also induces a transition from the open-ring amide form to the closed-ring spirolactam form; thereby, Cy-R6G gradually reverts to its hydrophobic state, which reduces the intensity of the absorption peak [33,41]. It is noteworthy that the rate of CO_2 removal from Cy-R6G via N_2 bubbling is much faster than the rate of the reaction between Cy-R6G and CO_2, demonstrating that the structure of CO_2-treated Cy-R6G is highly sensitive to changes in the surrounding environment and that CO_2-treated Cy-R6G is prone to dissociation of Cy-R6G. Similarly, after 60 min of N_2 bubbling, the ζ potential of the CO_2-treated Cy-R6G solution decreased from 37.89 ± 1.87 mV to nearly neutral (3.02 ± 0.14 mV), once again confirming that N_2 bubbling effectively restores CO_2-treated Cy-R6G to its original hydrophobic state. Similarly to N_2 bubbling, changing the ambient temperature (4, 25, and 50 °C) altered the removal of CO_2 from Cy-R6G. As shown in Fig. S11, the intensity of the maximum absorption and emission peaks decreased more rapidly over time at higher temperatures, clearly indicating that elevated temperatures accelerate the release or dissociation of CO_2 from CO_2-treated Cy-R6G, which eventually reverts to its original hydrophobic state. Furthermore, based on the N_2 bubbling data (Fig. 1f), the CO_2 release rate not only positively correlates with the ambient temperature, but N_2 bubbling treatment also simultaneously accelerates CO_2 release. Subsequently, to further understand the reversible binding and dissociation stability of Cy-R6G with CO_2, we investigated the reversible absorption characteristics of Cy-R6G aqueous solutions under alternating CO_2 and N_2 bubbling treatments using UV–Vis spectroscopy. As shown in Fig. 1g, Cy-R6G aqueous solution exhibited stable and reversible responses to CO_2 and N_2 after five cycles of 60 min of CO_2 bubbling followed by 15 min of N_2 bubbling at 25 °C, i.e., the absorption intensity alternately switched between approximately 0.22 and 0.05 after each cycle of CO_2 and N_2 bubbling. These results confirm that Cy-R6G aqueous solution undergoes stable hydrophilic/hydrophobic structural transitions on alternating CO_2 and N_2 bubbling, which is consistent with the macroscopic phenomena of switching between a pink solution and precipitate on CO_2 and N_2 bubbling, respectively (see inset on the left side of Fig. 1g and detailed in **Supplementary Video S1**). Therefore, these findings confirm that the cytosine moiety within the structure of Cy-R6G can react with and dissociate from CO_2, which profoundly affects the structural switching and photophysical properties of Cy-R6G.

Supplementary data related to this article can be found online at https://doi.org/10.1016/j.mtbio.2024.101319

After confirming the CO_2-responsive characteristics of Cy-R6G, we subsequently extended our research to encapsulation of Cy-R6G in Cy-PEG. Due to the ability of Cy-PEG to form stable spherical nanogels in aqueous environments (Fig. S12) [30], and considering that both structures contain cytosine groups which may enhance their affinity and interactions (Fig. 2a), we anticipated that Cy-PEG nanogels would successfully encapsulate hydrophobic Cy-R6G and exhibit desirable physical properties. Therefore, we first evaluated the encapsulation efficiency and structural characteristics of Cy-PEG nanogels physically encapsulating Cy-R6G by mixing and dialyzing Cy-R6G and Cy-PEG in an aqueous solution. As shown in Table S2 and Fig. 2b, the average diameter and drug loading content (DLC) of the Cy-PEG mixed system loaded with Cy-R6G gradually increased with the feed ratio of Cy-R6G. When the mixing ratio of Cy-R6G to Cy-PEG was 1.5:1, the resulting composite had an average diameter of 193 ± 6.79 nm and a DLC of 73.87 ± 1.97 %. These results indicate that the DLC and the size of the composite can be tailored by adjusting the mixing ratio of Cy-PEG and Cy-R6G to achieve the desired properties, possibly as the hydrogen bonding interactions between the cytosine groups of both components (Fig. 2a) [30,32] lead to high, tunable DLC values. In comparison, the control R6G-loaded Cy-PEG system achieved a maximum DLC of only 17.52 ± 1.56 % (Table S2), further demonstrating the importance of the cytosine groups in Cy-R6G and Cy-PEG. In addition, compared to the unloaded Cy-PEG nanogels with ζ values of 6.31 ± 5.26 mV, the ζ values of the Cy-R6G-loaded Cy-PEG composites in water ranged from −26 and −35 mV (depending on the DLC), confirming that encapsulation of Cy-R6G within Cy-PEG significantly enhances the high negative surface charge and structural stability of the nanogels [42]. Thus, the Cy-R6G-loaded Cy-PEG composites have a negative surface charge and tend to repel each other, which effectively prevents aggregation in aqueous solution. In confirmation of the co-organized structure of the composites in water, SEM and atomic force microscopy (AFM) images (Fig. 2c and d) clearly showed that the Cy-R6G-loaded Cy-PEG composites exhibited a well-dispersed morphology and spherical-like structures with diameters ranging from 75 to 110 nm, significantly larger than pristine Cy-PEG (Fig. S12). These observations confirmed that Cy-R6G was successfully encapsulated within the Cy-PEG nanogels and thereby increased the particle size. However, the average diameters observed in the SEM and AFM images are smaller than the results obtained by DLS (Fig. 2b), similarly to previous observations (right inset of Fig. 1e); this difference can be attributed to the effects of sample drying [38]. Overall, these findings demonstrate that the self-complementary hydrogen bonding interactions between cytosine groups in the Cy-R6G/Cy-PEG drug/carrier system enable the construction of nanospheres in aqueous solution with unique, tailorable physical properties.

Above, we successfully demonstrated that cytosine-functionalized Cy-R6G undergoes a sensitive and rapid response to CO_2 in aqueous solution, which induces a structural transition from hydrophobic to hydrophilic. Thus, we predicted that the Cy-R6G-loaded Cy-PEG nanogels would exhibit triggered drug release properties in CO_2-rich aqueous solutions due to the presence of CO_2-responsive Cy-R6G within the nanogels (i.e., due to formation of CO_2-protonated Cy-R6G inside the nanogels), which would ultimately confer precise and controllable drug release characteristics. Therefore, we explored the time-dependent effects of CO_2 bubbling on the macroscopic behavior of Cy-R6G-loaded Cy-PEG nanogels in aqueous solution. The photos in the top right corner of Fig. 2e and f, as well as **Supplementary Video S2**, clearly show that after 75 min of CO_2 bubbling at 25 °C, the color of the Cy-R6G-loaded Cy-PEG nanogels in water changed from colorless to pink while the solution remained clear and transparent, and exhibited yellow-green fluorescence under broad-spectrum UV light. These results indicate that CO_2 bubbling led to protonation of the cytosine and amine groups of Cy-R6G, and the resulting hydrophilic Cy-R6G was quickly released from the nanogels, leading to a macroscopically pink solution. Similar trends were observed for pH and ζ: after 75 min of CO_2 bubbling, the pH and ζ values of the Cy-R6G-loaded Cy-PEG nanogels in water changed from 7.21 ± 0.19 to 5.54 ± 0.31 and from −32.71 ± 2.40 to 16.33 ± 5.57

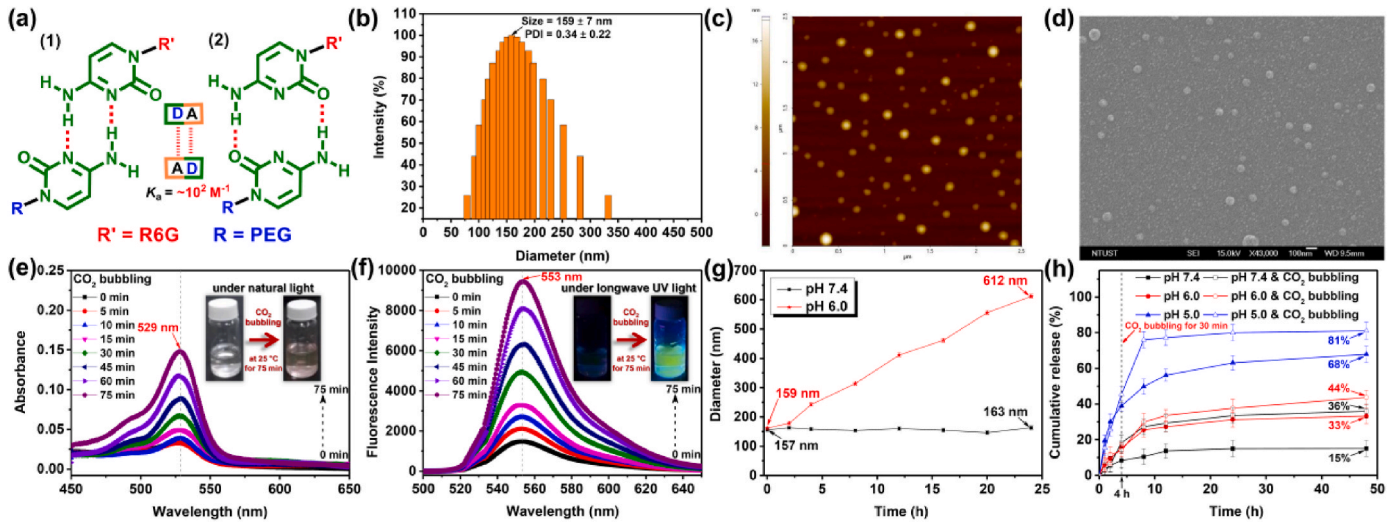

Fig. 2. **(a)** Formation of self-complementary hydrogen-bonded dimers between the cytosine moieties in Cy-R6G and Cy-PEG. **(b)** DLS curve of Cy-R6G-loaded Cy-PEG (1/1 Cy-R6G/Cy-PEG weight ratio) in aqueous solution recorded at 25 °C. **(c)** AFM and **(d)** SEM images of spin-coated Cy-R6G-loaded Cy-PEG nanogels. **(e)** UV–Vis and **(f)** PL spectra of Cy-R6G-loaded Cy-PEG in aqueous solution obtained at 25 °C after different durations of CO_2 bubbling (0–75 min). The top-left insets in **(e)** and **(f)** show photographs of Cy-R6G-loaded Cy-PEG nanogels in aqueous solution under natural light and long-wavelength UV light illumination before and after 75 min of CO_2 bubbling, respectively. **(g)** Time-dependent changes in the average sizes of Cy-R6G-loaded Cy-PEG in aqueous solutions at pH 7.4 and 5.0 obtained by DLS at 25 °C. **(h)** Drug release profiles of Cy-R6G-loaded Cy-PEG nanogels in aqueous solutions at pH 7.4, 6.0, and 5.0 at 25 °C with/without CO_2 bubbling. CO_2 bubbling was performed for 30 min, 4 h after the start of the drug release assay.

mV, respectively, confirming that CO_2 bubbling can rapidly and controllably trigger the release of Cy-R6G from the nanogels. Furthermore, UV–Vis and PL spectroscopy were employed to quantify the effects of the duration of CO_2 bubbling on the photophysical properties of Cy-R6G-loaded Cy-PEG nanogels in water. As shown in Fig. 2e and f, the maximum absorption and fluorescence peaks of Cy-R6G-loaded Cy-PEG nanogels at 529 and 553 nm, respectively, gradually increased from 0.03 to 1513 to 0.15 and 9570 during continuous CO_2 bubbling for 75 min, demonstrating that the Cy-PEG nanogels exhibit time-dependent drug release behavior. In contrast, no significant changes were observed in the UV–Vis spectra of Cy-R6G-loaded Cy-PEG nanogels in water after continuous N_2 bubbling for 60 min (Fig. S13), indicating that the Cy-R6G-loaded nanogels exhibit a highly selective response to CO_2 and demonstrating the high stability of Cy-R6G entrapped within the nanogels during N_2 bubbling. In comparison, no changes in the position and intensity of the characteristic peaks in the UV–Vis and PL spectra of control R6G-loaded Cy-PEG nanogels in water were observed after continuous CO_2 bubbling for 60 min (Fig. S14), clearly revealing that the presence of Cy-R6G is an indispensable factor that endows the nanogels with CO_2 responsiveness. Therefore, these intriguing findings inspired us to further explore the drug release behavior and kinetics of Cy-R6G-loaded Cy-PEG nanogels in aqueous environments in response to pH and CO_2.

Since CO_2 bubbling not only promotes a reaction with Cy-R6G but also increases the acidity of the aqueous solution, we examined the average particle sizes of Cy-R6G-loaded Cy-PEG nanogels at 25 °C in aqueous solutions of pH 7.4 and 6.0 through time-dependent DLS measurements. As shown in Fig. 2g, the particle size of Cy-R6G-loaded Cy-PEG nanogels in pH 7.4 aqueous solution remained almost unchanged, whereas the particle size of Cy-R6G-loaded Cy-PEG nanogels at pH 6.0 gradually increased from 159 nm at the beginning to 612 nm after 24 h. These results indicate that the self-complementary hydrogen bonding interactions between cytosine groups of Cy-R6G and Cy-PEG effectively enhance the structural stability of the nanogels under normal physiological conditions (Fig. 2a). In contrast, the hydrogen-bonded cytosine groups within the nanogels gradually dissociate in a weakly acidic aqueous environment, ultimately leading to structural disintegration of the nanogels and the subsequent release of Cy-R6G, which forms large aggregates. Therefore, this newly developed drug-delivery nanogel system based on CO_2-sensitive Cy-R6G and pH-responsive Cy-PEG has the potential to achieve precise and controllable drug delivery and release characteristics and thus enhance the safety and efficacy of cancer treatment [18,43]. Next, we explored the drug release kinetics of Cy-R6G-loaded Cy-PEG nanogels by evaluating the release behavior of Cy-R6G under different pH conditions and CO_2 bubbling using a typical dialysis method. As shown in Fig. 2h, Cy-PEG nanogels exhibited stable Cy-R6G encapsulation at 25 °C and pH 7.4, releasing only 15 % of the Cy-R6G after 48 h. However, at pH 6.0 and 5.0, the amount of Cy-R6G released significantly increased to 33 % and 68 %, respectively, after 48 h, confirming that Cy-R6G-loaded Cy-PEG is highly pH-responsive. The stability of the co-assembled structures under normal conditions and structural disintegration and release of Cy-R6G under acidic conditions can be attributed to the effects of environmental pH on the self-complementary hydrogen bonding interactions between the cytosine groups within the nanogels [30,32]. Surprisingly, the cumulative release of Cy-R6G from Cy-PEG nanogels over 48 h significantly increased after incubation in different pH environments for 4 h followed by CO_2 bubbling for 30 min, reaching 36 %, 44 %, and 81 % at pH values of 7.4, 6.0, and 5.0, respectively. This indicates that the nanogels undergo gradual disassembly due to the influence of CO_2, which subsequently promotes the conversion of Cy-R6G into its CO_2-protonated form, and thereby accelerates the release rate and increases the cumulative amount of Cy-R6G released from the disassembled nanogels. These observations further demonstrate that Cy-R6G-loaded Cy-PEG nanogels possess unique synergistic pH and CO_2 responsiveness, which could minimize the effects of the drug in normal tissues and enable enhanced controlled drug release in the tumor microenvironment, which typically has a mildly acidic and high CO_2 levels [18,44]. To verify the drug release kinetics, we further evaluated the particle size and morphological changes of Cy-R6G-loaded Cy-PEG nanogels after CO_2 bubbling for 75 min in pH 5.0 aqueous solution. As shown in Fig. S15, compared to the spherical Cy-R6G-loaded Cy-PEG nanogels in normal aqueous solution, DLS and SEM revealed a wide distribution of particle sizes and a morphology indicative of large aggregates, respectively, once again demonstrating that Cy-R6G-loaded Cy-PEG nanogels possess sensitive pH- and CO_2-responsive capabilities that lead to rapid disassembly and transformation into disordered aggregates in acidic and CO_2 aqueous environments. Based on these results, this Cy-R6G/Cy-PEG

drug/carrier system with dual pH- and CO_2-responsive capabilities holds great potential to enhance the stability of drug delivery and achieve more precisely controlled drug release in the tumor microenvironment.

An ideal drug delivery system must exhibit high structural stability in biological media to be safe for various biological applications [45]. Therefore, we conducted *in vitro* quantitative hemolysis assays of pristine Cy-R6G, Cy-PEG, and Cy-R6G-loaded Cy-PEG nanogels using sheep red blood cells (SRBC). As shown in the photographs in Fig. S16a and the qualitative analysis in Fig. S16b, the percentage of hemolysis of SRBC treated with Cy-PEG or Cy-R6G-loaded Cy-PEG nanogels in the concentration range of 0.1–100 μg/mL was below 3.1 %. However, the percentage of hemolysis increased gradually with the concentration of Cy-R6G, reaching the highest level of 14.9 ± 3.1 % at 100 μg/mL Cy-R6G. These results clearly reveal that the highly hydrophobic Cy-R6G is tightly encapsulated within the Cy-PEG nanogels, which effectively prevents lysis of SRBC, resulting in the desired anti-hemolytic properties and indicating the high potential of the nanogel for biomedical applications [46].

Next, to further understand whether Cy-R6G-loaded Cy-PEG nanogels with CO_2-responsive cytosine groups can selectively induce cytotoxicity in CO_2-rich microenvironments [32], we used the 3-(4, 5-dimethylthiazol-2-yl)-2,5-diphenyltetrazolium bromide (MTT) assay to assess the effects of pristine Cy-R6G and co-assembled Cy-R6G/Cy--PEG complexes on the viability of normal NIH/3T3 fibroblasts and HeLa cervical cancer cells in culture media in the presence or absence of CO_2. Before conducting the MTT assay, CO_2 was bubbled directly into the culture medium (Dulbecco's Modified Eagle Medium, DMEM) for 1 h to produce CO_2-containing DMEM, which temporarily remained saturated with CO_2. The pH of DMEM decreased from 7.8 ± 0.1 to 6.3 ± 0.1 after CO_2 bubbling treatment at 25 °C (Fig. S17). After standing for 1 day, the pH value of the solution rose to 6.8 ± 0.2, indicating that although the CO_2 content of the solution significantly decreased after 1 day, enough CO_2 was still present in the solution to establish a CO_2-rich culture environment for *in vitro* experiments. Subsequently, NIH/3T3 and HeLa cells were cultured in pristine or CO_2-containing DMEM at 37 °C for 24 h. The MTT assay showed that both cells exhibited over 98 % cell viability, indicating that the CO_2-containing DMEM environment did not affect the growth and viability of either type of cell (the gray bars on the far left in Fig. 3a and b), indicating that CO_2-containing DMEM was a suitable medium for subsequent *in vitro* experiments.

Additional MTT assays showed that co-incubation with Cy-R6G within the concentration range of 0.1–50 μg/mL in pristine DMEM at 37 °C for 24 h did not alter the cell viability of NIH/3T3 or HeLa cells (Fig. 3a and b), possibly as the hydrophobic nature of Cy-R6G results in low affinity with the cells, making it difficult for Cy-R6G to be taken up by the cells. Conversely, in the mildly acidic environment of CO_2-containing DMEM, Cy-R6G exhibited cytotoxic activity against NIH/3T3 and HeLa cells with half-maximal inhibitory concentration (IC_{50}) values of 37.5 μg/mL and 24.4 μg/mL, respectively. Thus, the acidic CO_2-containing culture environment effectively promoted transformation of Cy-R6G from a hydrophobic to a hydrophilic CO_2-protonated structure, and thereby significantly enhanced its uptake by cells and the subsequent induction of cytotoxicity. Surprisingly, Cy-R6G-loaded Cy-PEG nanogels led to completely different results compared to pristine Cy-R6G. Regardless of whether they were co-incubated with pristine DMEM or CO_2-containing DMEM for 24 h, NIH/3T3 cells treated with Cy-R6G-loaded Cy-PEG nanogels consistently showed high cell viability (Fig. 3a). These results suggest that the self-complementary hydrogen bonding between cytosine groups within the nanogel structure stably encapsulated Cy-R6G within Cy-PEG in the environment of normal cells, and thereby effectively prevented the sudden release of Cy-R6G from the nanogels, even in the CO_2-containing media. In contrast to normal NIH/3T3 cells, the viability of HeLa cancer cells incubated with Cy-R6G-loaded Cy-PEG nanogels in pristine DMEM for 24 h gradually decreased with the nanogel concentration, with an IC_{50} value of 25.3 μg/mL (Fig. 3b). This confirms that Cy-PEG nanogels effectively deliver Cy-R6G and confer selective cytotoxicity against HeLa cancer cells. These unique results can be attributed to two possible factors: Firstly, the self-complementary hydrogen bonding interactions between Cy-R6G and Cy-PEG form hydrogen-bonded cytosine dimers (Fig. 2a) that are prone to dissociation in the mildly acidic environment of HeLa cancer cells [44,47], which would lead to disassembly of the nanogels and the gradual release of Cy-R6G inside the cancer cells. Secondly, due to the presence of cytosine receptors on the surface of HeLa cells [32], Cy-R6G-loaded Cy-PEG nanogels may be selectively taken up by HeLa cells, which would enhance the degree of cellular internalization and confer targeted therapeutic efficacy. Thus, the nanogels selectively promote potent cytotoxic effects in HeLa cancer cells but do not affect the viability of healthy NIH/3T3 cells [18,44]. When the culture medium was changed to CO_2-containing DMEM, Cy-R6G-loaded Cy-PEG nanogels not only maintained their selective cytotoxicity against HeLa cells, but the IC_{50} value significantly reduced to 4.5 μg/mL (Fig. 3a and b). This indicates that after the nanogels are taken up by HeLa cells, the Cy-R6G released from the disassembled nanogels rapidly reacts with CO_2 to form hydrophilic CO_2-protonated Cy-R6G, which enhances the cytotoxicity of Cy-R6G towards HeLa cells. These results also suggest that the presence

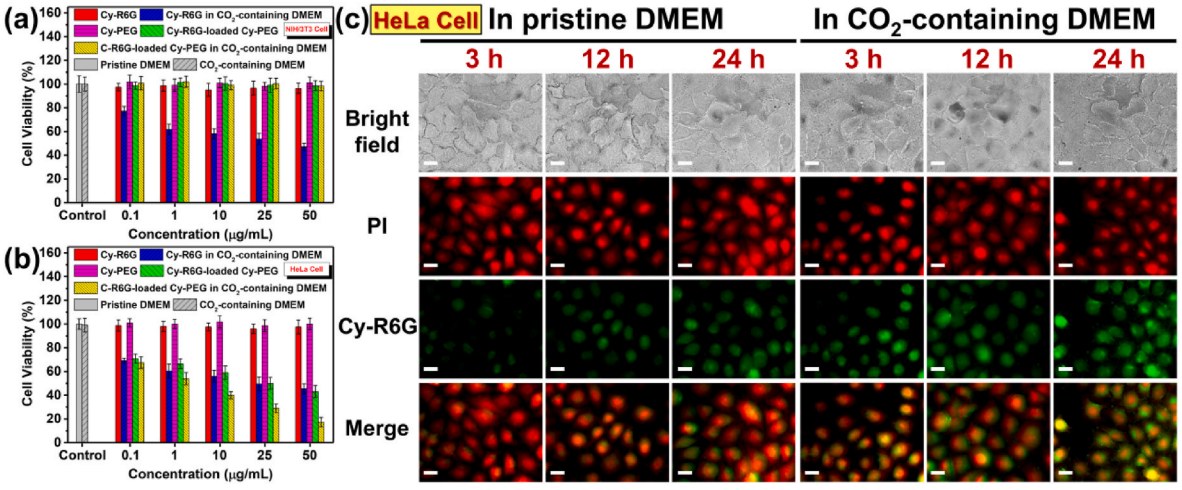

Fig. 3. In vitro viability of **(a)** NIH/3T3 and **(b)** HeLa cells after incubation with different concentrations of Cy-R6G, Cy-PEG, or Cy-R6G-loaded Cy-PEG nanogels in pristine or CO_2-containing DMEM at 37 °C for 24 h. **(c)** CLSM images of HeLa cells incubated with Cy-R6G-loaded Cy-PEG nanogels in pristine or CO_2-containing DMEM at 37 °C for 3, 12, or 24 h. The white scale bar in each image represents 20 μm.

of CO_2 in the medium may accelerate the selective uptake of R6G-loaded Cy-PEG nanogels by HeLa cells through cytosine receptor-mediated macropinocytosis, and thereby subsequently enhance the overall cancer cell killing efficacy [32,48]. Moreover, these findings also suggest that the combination of CO_2 and cytosine-induced selective cell internalization may confer a synergistic therapeutic effect to simultaneously achieve both accelerated and enhanced selective cytotoxicity against cancer cells.

These findings further motivated us to explore the enhanced selective cytotoxicity of Cy-R6G-loaded Cy-PEG nanogels towards HeLa cancer cells in pristine or CO_2-containing culture medium. We used propidium iodide (PI) staining and confocal laser scanning microscopy (CLSM) to observe uptake of Cy-R6G-loaded Cy-PEG nanogels by NIH/3T3 and HeLa cells over time when co-cultured in either pristine or CO_2-containing DMEM. PI staining causes cellular nuclei to exhibit red emission, while Cy-R6G-loaded Cy-PEG nanogels exhibit inherent faint green emission. As shown in Figs. S18 and 3c, the green emission of Cy-R6G-loaded Cy-PEG nanogels was not observed in NIH/3T3 cells during 24-h co-culture in either pristine or CO_2-containing DMEM, whereas green emission was detected within HeLa cells and the intensity of emission increased over time. These results suggest that Cy-R6G-loaded Cy-PEG nanogels may not be taken up by NIH/3T3 cells because the surface of normal cells is neutral or slightly positively charged [49]. In contrast, due to the presence of cytosine receptors on the surface of HeLa cancer cells [32], a high affinity interaction between the nanogels and HeLa cells promotes selective internalization and accumulation of the nanogels inside HeLa cells through cytosine receptor-mediated macropinocytosis [50,51]. The CLSM images are consistent with and support the results of the MTT assay (Fig. 3a and b). In the merged images in Fig. 3c, if Cy-R6G-loaded Cy-PEG nanogels are internalized within the HeLa cells, their green emission overlapped with the blue emission of the cell nuclei, resulting in bright yellow emission. Surprisingly, at different time points, the intensity of the yellow emission within HeLa cells treated in CO_2-containing DMEM was substantially higher than in the cells treated in pristine DMEM. After 24 h, yellow emission was uniformly distributed throughout each cell treated in CO_2-containing DMEM, suggesting that a reaction between the Cy-R6G within the nanogels and CO_2 (resulting in hydrophilic CO_2-protonated Cy-R6G), altered the surface charge of the nanogels and in turn significantly accelerated the cellular uptake and enhanced the accumulation of the nanogels within HeLa cells. In other words, the combination of CO_2-sensitive Cy-R6G and pH-responsive Cy-PEG, along with specific targeting of the cytosine groups on cancer cells, may crucially enhance the efficacy and safety of chemotherapeutic treatment.

To further validate the CLSM results, we qualitatively and quantitatively analyzed cellular internalization of Cy-R6G-loaded Cy-PEG

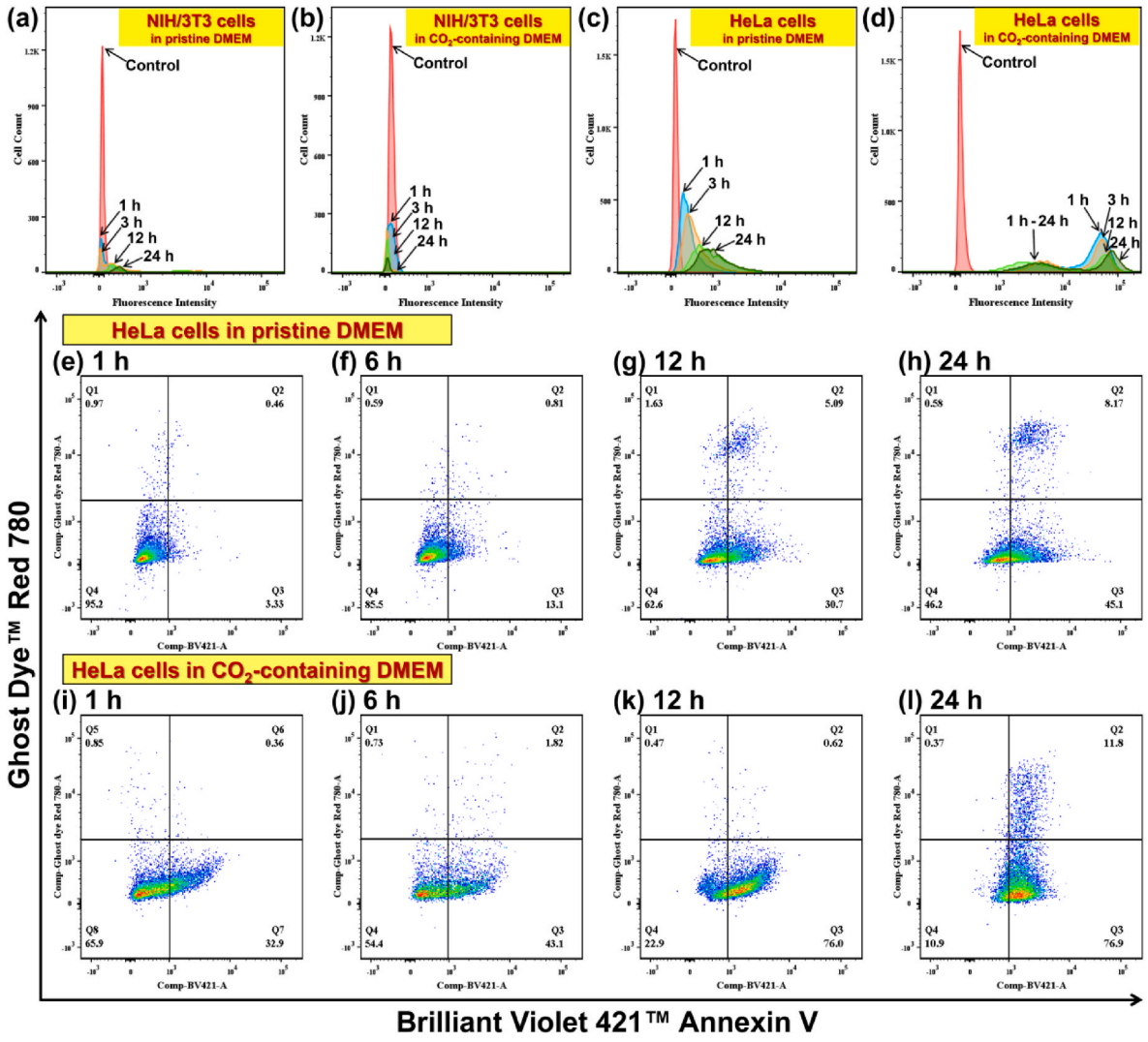

Fig. 4. Representative flow cytometry histograms of **(a, b)** NIH/3T3 and **(c, d)** HeLa cells incubated with Cy-R6G-loaded Cy-PEG nanogels in pristine or CO_2-containing DMEM at 37 °C for 3, 12, or 24 h. Representative flow cytometry histogram of HeLa cells incubated with Cy-R6G-loaded Cy-PEG nanogels at 37 °C for 1, 6, 12, or 24 h in **(e–h)** pristine DMEM or **(i–l)** CO_2-containing DMEM. Cells were stained with BV421 Annexin V and GDR780 prior to flow cytometry analysis.

nanogels in NIH/3T3 and HeLa cells using flow cytometry. After co-culture in pristine or CO_2-containing DMEM for 24 h, Cy-R6G-loaded Cy-PEG nanogels exhibited almost no characteristic fluorescence signal of Cy-R6G in NIH/3T3 cells (Fig. 4a and b). In contrast, the fluorescence intensity in HeLa cells treated with Cy-R6G-loaded Cy-PEG increased over time in both pristine and CO_2-containing DMEM (Fig. 4c and d), clearly suggesting that HeLa cells exhibited highly selective uptake of Cy-R6G-loaded Cy-PEG nanogels. This further confirms that the surface of HeLa cells possesses cytosine receptors that facilitate selective internalization of Cy-PEG nanogels [32]. More importantly, compared to cells treated with the nanogels in pristine DMEM, the CO_2-containing DMEM environment altered the surface charge of Cy-R6G-loaded Cy-PEG nanogels, which accelerated their internalization and ultimately resulted in a faster uptake rate and higher accumulation of Cy-R6G-loaded nanogels within the HeLa cells. In addition, HeLa cells treated with Cy-R6G-loaded Cy-PEG in CO_2-containing DMEM exhibited a bimodal distribution, which may be attributed to varying degrees of reaction between the nanogels and CO_2 resulting in different distributions of fluorescence intensity within the cells. Quantitative comparison of fluorescence intensities (Fig. 4a–d, summarized in Fig. S19) indicated that in CO_2-containing DMEM, the fluorescence intensity of HeLa cells treated with Cy-R6G-loaded Cy-PEG reached approximately 25,600 after 1 h of co-culture and increased to about 41,000 after 24 h. In contrast, in pristine DMEM, the fluorescence intensity of HeLa cells treated with Cy-R6G-loaded Cy-PEG only reached ~1500 after 24 h of co-culture; at this time point, the fluorescence intensity of HeLa cells treated with Cy-R6G-loaded Cy-PEG in CO_2-containing DMEM was more than 27 times higher than the cells treated with Cy-R6G-loaded Cy-PEG in pristine DMEM. These results further confirm that the presence of CO_2 in the DMEM significantly accelerates the internalization of Cy-PEG nanogels by HeLa cells. Overall, these observations strongly indicate that the selective tumor cell-targeting characteristics and CO_2 responsiveness of the cytosine groups are critical factors that facilitate accelerated internalization of the Cy-R6G/Cy-PEG system into cancer cells and enhance its selective cytotoxic properties, thus this novel system may potentially offer a safer and more effective pathway for cancer therapy.

To further confirm the potential mechanisms of cell death in HeLa cancer cells, we subsequently performed quantitative analysis using flow cytometry combined with Brilliant Violet 421™ Annexin V (BV421 Annexin V) and Ghost Dye™ Red 780 (GDR780) double staining to determine the proportions of healthy, necrotic, and apoptotic cells after co-culture of Cy-R6G-loaded Cy-PEG nanogels with NIH/3T3 and HeLa cells in pristine or CO_2-containing DMEM. The combination of BV421 Annexin V and GDR780 is widely used to detect differences in cell membrane permeability [52,53]. As shown in Fig. 4e-l and S20, the BV421 Annexin V/GDR780 system can be used to quantify healthy cells (lower left quadrant, BV421 Annexin V negative/GDR780 negative), early apoptotic cells (lower right quadrant, BV421 Annexin V positive/GDR780 negative), late apoptotic cells (upper right quadrant, BV421 Annexin V positive/GDR780 positive), and necrotic cells (upper left quadrant, BV421 Annexin V negative/GDR780 positive). As shown in Fig. S20, regardless of whether they were cultured in pristine or CO_2-containing DMEM for 24 h, over 88 % of NIH/3T3 cells co-cultured with Cy-R6G-loaded Cy-PEG remained healthy, indicating that Cy-PEG nanogels encapsulate Cy-R6G in a highly stable manner, which effectively prevents disintegration of the nanogels and uncontrolled drug release, even in a CO_2-containing DMEM environment. In contrast, during co-culture of Cy-R6G-loaded Cy-PEG nanogels with HeLa cells in pristine DMEM, the initially healthy HeLa cells gradually transitioned to apoptotic cells over time. This indicates that the HeLa cells selectively internalized the Cy-R6G-loaded Cy-PEG nanogels and the acidic intracellular environment gradually lead to disassembly of the nanogels and the subsequent release of Cy-R6G. Specifically, after co-culture with Cy-R6G-loaded Cy-PEG in pristine DMEM for only 1 h, over 95 % of HeLa cells remained viable (Fig. 4e), suggesting that the presence of cytosine receptors on the surface of HeLa cells enhances the affinity between the nanogels and the cells and leads to gradual macropinocytosis of the nanogels [32]. When the duration of co-culture was extended to 24 h, the proportion of healthy HeLa cells drastically decreased to 46 %, while the proportions of early and late apoptotic cells increased to 45 % and 8 %, respectively; only about 0.6 % of cells were necrotic (Fig. 4h). This positively demonstrates that Cy-R6G-loaded Cy-PEG nanogels undergo selective uptake and induce high levels of apoptosis in HeLa cells, and can ultimately achieve the desired chemotherapeutic effect [54]. Surprisingly, when DMEM was replaced with CO_2-containing DMEM, the rate at which Cy-R6G-loaded Cy-PEG nanogels induced apoptosis in HeLa cells increased significantly (Fig. 4i-l). After just 1 h of incubation in the CO_2-containing DMEM, the proportion of healthy HeLa cells decreased to 66 %, with about 33 % of early apoptotic cells (Fig. 4i). At 6 h, the proportion of early apoptotic cells further increased to 43 % (Fig. 4j), revealing that the CO_2-containing microenvironment not only accelerated internalization of the Cy-R6G-loaded Cy-PEG nanogels into HeLa cells, but also that the CO_2 and weakly acidic cancer cell environment accelerated disassembly of the nanogels and enhanced the cytotoxic effects of Cy-R6G, leading to rapid induction of apoptosis. Ultimately, after 24 h of incubation, the proportions of early and late apoptotic cells increased to 77 % and 12 %, respectively, while only about 11 % of remained cells healthy, with almost no necrotic cells (Fig. 4l). This further demonstrates that, compared to the pristine DMEM, the CO_2-containing DMEM effectively enhances the rate and extent of apoptosis induced by Cy-R6G-loaded Cy-PEG nanogels in HeLa cancer cells by the same cytotoxic pathway and mechanism.

Collectively, compared to traditional drug delivery systems, this novel CO_2 and pH-responsive system based on a combination of Cy-R6G and Cy-PEG offers three unique advantages that may effectively enhance the safety and efficacy of cancer chemotherapy [7,55]: Firstly, hydrophobic Cy-R6G and hydrophilic Cy-PEG co-assemble into nanogels through self-complementary hydrogen bonding between their cytosine groups, which not only significantly enhances the solubility of Cy-R6G in aqueous environments but also improves its structural stability in biological environments. Secondly, the Cy-R6G-loaded Cy-PEG nanogels can be tailored to precisely control the release characteristics of Cy-R6G in hypercapnic and slightly acidic cancer cell environments. Thirdly, due to the high structural stability of Cy-R6G-loaded Cy-PEG nanogels in normal cellular environments and the high affinity and specific interaction of the nanogels with the surface of cancer cells, the nanogels undergo significantly faster and higher degrees of selective internalization by cancer cells in CO_2-containing culture media. Thus, Cy-R6G-loaded Cy-PEG can induce extensive levels of apoptosis in cancer cells without affecting the vitality of normal cells, and thus may help to achieve safer, more effective cancer treatment through a cytotoxic pathway. Therefore, this emerging CO_2-responsive drug delivery system opens up new opportunities to significantly enhance selective uptake of chemotherapy drugs by cancer cells and accelerate the induction of apoptosis, and thus also demonstrates high potential to improve the overall efficacy of cancer treatment.

4. Conclusions

In summary, this study presents a facile and efficient approach to establish a CO_2-responsive multifunctional supramolecular drug delivery system that could enhance the safety, reliability, and efficacy of chemotherapy. The system is based on self-complementary multiple hydrogen bonding between cytosine groups to obtain a combination of CO_2-responsive Cy-R6G as a hydrophobic anticancer agent and pH-sensitive Cy-PEG as a hydrophilic nanocarrier. Cy-R6G and Cy-PEG are synthesized through simple, few-step pathways at high yield and quality. Due to the self-complementary hydrogen bonding interactions between cytosine groups in their structures, Cy-R6G and Cy-PEG co-assemble into a nanogel in aqueous environments and stably

encapsulate the hydrophobic Cy-R6G in solution. The Cy-R6G-loaded Cy-PEG nanogels have a widely tunable size and Cy-R6G loading capacity, ranging from 144 to 194 nm and 62–74 %, respectively, depending on the mixing ratio of Cy-R6G and Cy-PEG. The nanogels exhibit numerous unique physical properties, such as extremely high structural stability in normal aqueous environments, intriguing optical/emission phenomena, enhanced anti-hemolytic activity against SRBC, highly sensitive pH/CO_2 responsiveness, as well as stable and reversible structural and emission switching characteristics in aqueous solution in response to alternating CO_2/N_2 bubbling. MTT assays clearly indicated that, due to the presence of cytosine receptors on the surface of HeLa cancer cells, Cy-R6G-loaded Cy-PEG nanogels exhibit selective cytotoxicity towards HeLa cells in pristine DMEM, but have minimal impact on the viability of NIH/3T3 normal cells. Surprisingly, using CO_2-containing DMEM medium to simulate hypercapnic conditions significantly enhanced the cytotoxicity of Cy-R6G-loaded Cy-PEG nanogels towards HeLa cells compared to cells treated in pristine DMEM. This significant enhancement in cytotoxicity towards cancer cells, in addition to the specific targeting provided by cytosine receptors on the cancer cells, may also be due to the CO_2-rich microenvironment altering the surface charge of the nanogels, and thereby accelerating cellular uptake and rapid disassembly of Cy-PEG and the release of Cy-R6G in the weakly acidic microenvironment of cancer cells. Subsequently, the CO_2-protonated Cy-R6G confers a higher degree of selective cytotoxicity. The unique physical properties and significantly enhanced selective cytotoxicity towards cancer cells reveal that the targeting characteristics of the cytosine groups and the CO_2-responsive capabilities are crucial for achieving the desired anticancer therapeutic effects; to our knowledge, these characteristics are quite rare and highly anticipated compared to typical drug delivery systems. Importantly, cellular fluorescence imaging, flow cytometry, and investigations into the cytotoxic mechanisms confirmed that, compared to pristine DMEM, the culture environment of CO_2-containing DMEM not only accelerates the internalization of Cy-R6G-loaded Cy-PEG nanogels by cancer cells through cytosine-mediated macropinocytosis, but also subsequently leads to induction of massive levels of apoptosis following the intracellular release of Cy-R6G. Overall, this combination of CO_2-responsive Cy-R6G with pH-sensitive Cy-PEG significantly enhances the rate of selective cellular internalization of co-assembled nanogels into cancer cells in CO_2-containing DMEM and thereby efficiently accelerates the induction of apoptosis in cancer cells. Therefore, this research provides a safe, reliable, and highly promising approach for the development and application of CO_2-responsive multifunctional drug delivery systems in cancer chemotherapy.

Funding sources

This study was supported financially by the National Science and Technology Council, Taiwan (contract no. NSTC 110-2221-E−011-003-MY3 and 113-2221-E−011-007-MY3).

CRediT authorship contribution statement

Enyew Alemayehu Bayle: Validation, Methodology, Data curation. **Fasih Bintang Ilhami:** Validation, Methodology, Data curation. **Jem-Kun Chen:** Investigation. **Chih-Chia Cheng:** Writing – review & editing, Writing – original draft, Visualization, Supervision, Resources, Methodology, Investigation, Funding acquisition, Conceptualization.

Declaration of competing interest

The author(s) declare(s) that there is no conflict of interest regarding the publication of this article.

Acknowledgments

This study was supported financially by the National Science and Technology Council, Taiwan (contract no. NSTC 110-2221-E-011-003-MY3 and 113-2221-E-011-007-MY3). Flow cytometric cell sorting was performed on a BD FACSAria III system at the Technology Commons in College of Life Science in the Instrumentation Center sponsored by the National Science and Technology Council, National Taiwan University, with technical assistance provided by Ms. Wan-Shu Yao.

Appendix A. Supplementary data

Supplementary data to this article can be found online at https://doi.org/10.1016/j.mtbio.2024.101319.

Data availability

The authors do not have permission to share data.

References

[1] U. Anand, A. Dey, A.K. Singh Chandel, R. Sanyal, A. Mishra, D.K. Pandey, V. De Falco, A. Upadhyay, R. Kandimalla, A. Chaudhary, J.K. Dhanjal, S. Dewanjee, J. Vallamkondu, J.M.P. de la Lastrao, Cancer chemotherapy and beyond: current status, drug candidates, associated risks and progress in targeted therapeutics, Genes Dis 10 (2023) 1367–1401.

[2] N. Behranvand, F. Nasri, R.Z. Emameh, P. Khani, A. Hosseini, J. Garssen, R. Falak, Chemotherapy: a double-edged sword in cancer treatment, Cancer Immunol. Immunother. 71 (2022) 507–526.

[3] V. Schirrmacher, From chemotherapy to biological therapy: a review of novel concepts to reduce the side effects of systemic cancer treatment, Int. J. Oncol. 54 (2019) 407–419.

[4] R. Oun, Y.E. Moussa, N.J. Wheate, The side effects of platinum-based chemotherapy drugs: a review for chemists, Dalton Trans. 47 (2018) 6645–6653.

[5] V. Oliveri, Selective targeting of cancer cells by copper ionophores: an overview, Front. Mol. Biosci. 9 (2022) 841814.

[6] M. Shadidi, M. Sioud, Selective targeting of cancer cells using synthetic peptides, Drug Resist. Updat. 6 (2003) 363–371.

[7] J.K. Patra, G. Das, L.F. Fraceto, E.V.R. Campos, M.d.P. Rodriguez-Torres, L. S. Acosta-Torres, L.A. Diaz-Torres, R. Grillo, M.K. Swamy, S. Sharma, S. Habtemariam, H.-Se Shin, Nano based drug delivery systems: recent developments and future prospects, J. Nanobiotechnology 16 (2018) 71.

[8] J. Zhou, L. Rao, G. Yu, T.R. Cook, X. Chen, F. Huang, Supramolecular cancer nanotheranostics, Chem. Soc. Rev. 50 (2021) 2839–2891.

[9] M. Yan, S. Wu, Y. Wang, M. Liang, M. Wang, W. Hu, G. Yu, Z. Mao, F. Huang, J. Zhou, Recent progress of supramolecular chemotherapy based on host–guest interactions, Adv. Mater. 36 (2024) 2304249.

[10] X. Ma, H. Tian, Stimuli-responsive supramolecular polymers in aqueous solution, Acc. Chem. Res. 47 (2014) 1971–1981.

[11] M. Mrinalini, S. Prasanthkumar, Recent advances on stimuli-responsive smart materials and their applications, ChemPlusChem 84 (2019) 1103–1121.

[12] M.I. Khan, M.I. Hossain, M.K. Hossain, M.H.K. Rubel, K.M. Hossain, A.M.U. B. Mahfuz, M.I. Anik, Recent progress in nanostructured smart drug delivery systems for cancer therapy: a review, ACS Appl. Bio Mater. 5 (2022) 971–1012.

[13] S. Hossen, M.K. Hossain, M.K. Basher, M.N.H. Mia, M.T. Rahman, M.J. Uddin, Smart nanocarrier-based drug delivery systems for cancer therapy and toxicity studies: a review, J. Adv. Res. 15 (2018) 1–18.

[14] A.C. Selfridge, M.A.S. Cavadas, C.C. Scholz, E.L. Campbell, L.C. Welch, E. Lecuona, S.P. Colgan, K.E. Barrett, P.H.S. Sporn, J.I. Sznajder, E.P. Cummins, C.T. Taylor, Hypercapnia suppresses the HIF-dependent adaptive response to hypoxia, J. Biol. Chem. 291 (2016) 11800–11808.

[15] S. Zhang, Y. Yang, S. Liu, R. Dong, Z. Qian, Influence of the hypercapnic tumor microenvironment on the viability of HeLa cells screened by a CO_2-gradient-generating device, ACS Omega 6 (2021) 26773–26781.

[16] R. Kikuchi, Y. Iwai, T. Tsuji, Y. Watanabe, N. Koyama, K. Yamaguchi, H. Nakamura, K. Aoshiba, Hypercapnic tumor microenvironment confers chemoresistance to lung cancer cells by reprogramming mitochondrial metabolism in vitro, Free Radic. Biol. Med. 134 (2019) 200–214.

[17] A. Nevler, S.Z. Brown, D. Nauheim, C. Portocarrero, J. Bassig, C.W. Schultz, G. McCarthy, H. Lavu, T.P. Yeo, C.J. Yeo, J.R. Brody, Effect of hypercapnia, an element of obstructive respiratory disorder, on pancreatic cancer chemoresistance and progression, J. Am. Coll. Surg. 230 (2020) 659–667.

[18] R. Kumari, D. Sunil, R.S. Ningthoujam, Hypoxia-responsive nanoparticle based drug delivery systems in cancer therapy: an up-to-date review, J. Control. Release 319 (2020) 135–156.

[19] H.W. Yong, A. Kakkar, The unexplored potential of gas-responsive polymers in drug delivery: progress, challenges and outlook, Polym. Int. 71 (2022) 514–520.

[20] A. Darabi, P.G. Jessop, M.F. Cunningham, CO_2-responsive polymeric materials: synthesis, self-assembly, and functional applications, Chem. Soc. Rev. 45 (2016) 4391–4436.

[21] Y. Wang, S. Yang, J. Zhang, Z. Chen, B. Zhu, J. Li, S. Liang, Y. Bai, J. Xu, D. Rao, L. Dong, C. Zhang, X. Yang, Scalable and switchable CO_2-responsive membranes with high wettability for separation of various oil/water systems, Nat. Commun. 14 (2023) 1108.
[22] M.F. Cunningham, P.G. Jessop, Carbon dioxide-switchable polymers: where are the future opportunities? Macromolecules 52 (2019) 6801–6816.
[23] P.K.S. Magut, S. Das, V.E. Fernand, J. Losso, K. McDonough, B.M. Naylor, S. Aggarwal, I.M. Warner, Tunable cytotoxicity of rhodamine 6G via anion variations, J. Am. Chem. Soc. 135 (2013) 15873–15879.
[24] M. Barzan, F. Hajiesmaeilbaigi, Investigation the concentration effect on the absorption and fluorescence properties of Rhodamine 6G dye, Optik 159 (2018) 157–161.
[25] S. Zeng, X. Liu, Y.S. Kafuti, H. Kim, J. Wang, X. Peng, H. Li, J. Yoon, Fluorescent dyes based on rhodamine derivatives for bioimaging and therapeutics: recent progress, challenges, and prospects, Chem. Soc. Rev. 52 (2023) 5607–5651.
[26] N. Bhattarai, M. Chen, R.L. Pérez, S. Ravula, P. Chhotaray, S. Hamdan, K. McDonough, S. Tiwaric, I.M. Warner, Enhanced chemotherapeutic toxicity of cyclodextrin templated size-tunable rhodamine 6G nanoGUMBOS, J. Mater. Chem. B 6 (2018) 5451–5459.
[27] N. Bhattarai, J.M. Mathis, M. Chen, R.L. Pérez, N. Siraj, P.K.S. Magut, K. McDonough, G. Sahasrabudhe, I.M. Warner, Endocytic selective toxicity of rhodamine 6G nanoGUMBOS in breast cancer cells, Mol. Pharm. 15 (2018) 3837–3845.
[28] M. Kutushov, O. Gorelik, Low concentrations of Rhodamine-6G selectively destroy tumor cells and improve survival of melanoma transplanted mice, Neoplasma 60 (2013) 262–273.
[29] V.T.T. Ngan, P.Y. Chiou, F.B. Ilhami, E.A. Bayle, Y.T. Shieh, W.T. Chuang, J. K. Chen, J.Y. Lai, C.C. Cheng, A CO_2-responsive imidazole-functionalized fluorescent material mediates cancer chemotherapy, Pharmaceutics 15 (2023) 354.
[30] F.B. Ilhami, Y.T. Yang, A.W. Lee, Y.H. Chiao, J.K. Chen, D.J. Lee, J.Y. Lai, C. C. Cheng, Hydrogen bond strength-mediated self-assembly of supramolecular nanogels for selective and effective cancer treatment, Biomacromolecules 22 (2021) 4446–4457.
[31] F.B. Ilhami, S.Y. Huang, C.C. Cheng, Multi-biofunctional silver-containing metallosupramolecular nanogels for efficient antibacterial treatment and selective anticancer therapy, Acta Biomater. 151 (2022) 576–587.
[32] W.L. Fan, S.Y. Huang, X.J. Yang, F.B. Ilhami, J.K. Chen, C.C. Cheng, Hydrogen-bonded cytosine-endowed supramolecular polymeric nanogels: highly efficient cancer cell targeting and enhanced therapeutic efficacy, J. Colloid Interface Sci. 665 (2024) 329–344.
[33] H.N. Kim, M.H. Lee, H.J. Kim, J.S. Kim, J. Yoon, A new trend in rhodamine-based chemosensors: application of spirolactam ring-opening to sensing ions, Chem. Soc. Rev. 37 (2008) 1465–1472.
[34] S. Singha, Y.W. Jun, S. Sarkar, K.H. Ahn, An endeavor in the reaction-based approach to fluorescent probes for biorelevant analytes: challenges and achievements, Acc. Chem. Res. 52 (2019) 2571–2581.
[35] E.N. Nikolova, G.B. Goh, C.L. Brooks, H.M. Al-Hashimi, Characterizing the protonation state of cytosine in transient G·C Hoogsteen base pairs in duplex DNA, J. Am. Chem. Soc. 135 (2013) 6766–6769.
[36] D. Lee, K.M.K. Swamy, J. Hong, S. Lee, J. Yoon, Sens. A rhodamine-based fluorescent probe for the detection of lysosomal pH changes in living cells, Actuators B Chem 266 (2018) 416–421.
[37] J. Byun, W. Huang, D. Wang, R. Li, K.A.I. Zhang, CO_2-Triggered switchable hydrophilicity of a heterogeneous conjugated polymer photocatalyst for enhanced catalytic activity in water, Angew. Chem. Int. Ed. 57 (2018) 2967–2971.
[38] C.M. Hoo, N. Starostin, P.E. West, M.L. Mecartney, A comparison of atomic force microscopy (AFM) and dynamic light scattering (DLS) methods to characterize nanoparticle size distributions, J. Nanoparticle Res. 10 (2008) 89–96.
[39] Y.N. Hsiao, F.B. Ilhami, C.C. Cheng, CO_2-responsive water-soluble conjugated polymers as a multifunctional fluorescent probe for bioimaging applications, Biomacromolecules 25 (2024) 997–1008.
[40] Q. Zhang, G. Yu, W.J. Wang, H. Yuan, B.G. Li, S. Zhu, Preparation of N_2/CO_2 triggered reversibly coagulatable and redispersible latexes by emulsion polymerization of styrene with a reactive switchable surfactant, Langmuir 28 (2012) 5940–5946.
[41] H. Li, H. Guan, X. Duan, J. Hu, G. Wang, Q. Wang, An acid catalyzed reversible ring-opening/ring-closure reaction involving a cyano-rhodamine spirolactam, Org. Biomol. Chem. 11 (2013) 1805–1809.
[42] D.J. Pochapski, C.C. dos Santos, G.W. Leite, S.H. Pulcinelli, C.V. Santilli, Zeta potential and colloidal stability predictions for inorganic nanoparticle dispersions: effects of experimental conditions and electrokinetic models on the interpretation of results, Langmuir 37 (2021) 13379–13389.
[43] P. Mi, Stimuli-responsive nanocarriers for drug delivery, tumor imaging, therapy and theranostics, Theranostics 10 (2020) 4557–4588.
[44] L. Feng, Z. Dong, D. Tao, Y. Zhang, Z. Liu, The acidic tumor microenvironment: a target for smart cancer nano-theranostics, Natl. Sci. Rev. 5 (2018) 269–286.
[45] T.L. Moore, L. Rodriguez-Lorenzo, V. Hirsch, S. Balog, D. Urban, C. Jud, B. Rothen-Rutishauser, M. Lattuada, A. Petri-Fink, Nanoparticle colloidal stability in cell culture media and impact on cellular interactions, Chem. Soc. Rev. 44 (2015) 6287–6305.
[46] G. Jeswani, A. Alexander, S. Saraf, S. Saraf, A. Qureshi, Ajazuddin, Recent approaches for reducing hemolytic activity of chemotherapeutic agents, J. Control. Release 211 (2015) 10–21.
[47] W. Le, B. Chen, Z. Cui, Z. Liu, D. Shi, Detection of cancer cells based on glycolytic-regulated surface electrical charges, Biophys Rep 5 (2019) 10–11.
[48] L. Huang, S. Zhao, F. Fang, T. Xu, M. Lan, J. Zhang, Advances and perspectives in carrier-free nanodrugs for cancer chemo-monotherapy and combination therapy, Biomaterials 268 (2021) 120557.
[49] B. Chen, W. Le, Y. Wang, Z. Li, D. Wang, L. Ren, L. Lin, S. Cui, J.J. Hu, Y. Hu, P. Yang, R.C. Ewing, D. Shi, Z. Cui, Targeting negative surface charges of cancer cells by multifunctional nanoprobes, Theranostics 6 (2016) 1887–1898.
[50] J. Dausend, A. Musyanovych, M. Dass, P. Walther, H. Schrezenmeier, K. Landfester, V. Mailänder, Uptake mechanism of oppositely charged fluorescent nanoparticles in HeLa cells, Macromol, Biosci. 8 (2008) 1135–1143.
[51] P. Foroozandeh, A.A. Aziz, Insight into cellular uptake and intracellular trafficking of nanoparticles, Nanoscale Res. Lett. 13 (2018) 339.
[52] I. Vermes, C. Haanen, H. Steffens-Nakken, C. Reutelingsperger, A novel assay for apoptosis flow cytometric detection of phosphatidylserine expression on early apoptotic cells using fluorescein labelled annexin V, J. Immunol. Methods 184 (1995) 39–51.
[53] M.N. Van Engeland, L.J. Nieland, F.C. Ramaekers, B. Schutte, C. P. Reutelingsperger, Annexin V-affinity assay: a review on an apoptosis detection system based on phosphatidylserine exposure, Cytometry 31 (1998) 1–9.
[54] B.A. Carneiro, W.S. El-Deiry, Targeting apoptosis in cancer therapy, Nat. Rev. Clin. Oncol. 17 (2020) 395–417.
[55] M.J. Mitchell, M.M. Billingsley, R.M. Haley, M.E. Wechsler, N.A. Peppas, R. Langer, Engineering precision nanoparticles for drug delivery, Nat. Rev. Drug Discov. 20 (2021) 101–124.